PHILIPPINE ENGINEERING JOURNAL
PEJ 2014; Vol. 35, No. 1: 25-40

A NUMERICAL STUDY ON THE INFLUENCE OF SOLIDITY ON THE PERFORMANCE OF VERTICAL AXIS WIND TURBINES

Okeoghene Eboibi[1], Robert Howell[2]and Louis Angelo Danao[3]
[1]Department of Agricultural Engineering
Delta State Polytechnic, Ozoro, Nigeria
[2]Department of Mechanical Engineering
University of Sheffield, Sheffield, United Kingdom
[3]Department of Mechanical Engineering
University of the Philippines, Diliman, Quezon City, Philippines

ABSTRACT

Computational Fluid Dynamics has been used to test seven configurations of a 5kW three–bladed Vertical Axis Wind Turbine based on a NACA0012 profile. The turbine aerofoil chord has been changed to alter the turbine solidity and this has been tested over a wide range of tip speed ratios. Validation is based on comparison to tests on a pitching aerofoil, at a similar Reynolds number. The investigations determined how and why the change in aerofoil chord and therefore solidity affected the performance of the turbine. The aerofoil chord lengths investigated varied between 0.098m and 0.48m resulting in solidities of between 0.2 and 0.98. An energy yield analysis method was developed to determine the configuration of the turbine with best performance assuming the configurations operated over a Rayleigh wind distribution with an annual mean value of 6m/s. The results showed that the characteristics of the turbine map (Cp vs. λ) for a solidity of 0.3 were most favorable for the given wind distribution and resulted in the highest energy yield.

Keywords: *VAWT, CFD, solidity, energy yield analysis*

1. INTRODUCTION

The concerns over global warming and greenhouse gas effects of human activities have continued to grow in recent years. This has increased the need for formulation of policies by government, agencies, industry and individuals to improve renewable energy generation. This awareness and its consequent formulated policies are currently promoting interest in wind energy conversion systems and other renewable sources for energy generation. The UK government had set targets for renewable energy generation of 15% of UK energy consumption by 2020. This policy has contributed to the achievement of 45% of the UK's renewable energy generation from wind in 2011 [1].

Correspondence to: Louis Angelo Danao, Dept. of Mechanical Engineering, University of the Philippines, Diliman, Quezon City. Email: louisdanao@coe.upd.edu.ph.

Received: January 21, 2013
Accepted: May 21, 2014

Electricity generation from wind can be achieved by lift–based wind turbines classified as Horizontal Axis Wind Turbines (HAWTs) and Vertical Axis Wind Turbines (VAWTs) [2]. HAWTs are dominant for large scale energy generation because of many years of research attention they have attracted. While VAWTs have received little or no attention until the oil crisis of 1970 which re–invigorated research interest in many renewable energy conversion systems including the Darrieus and Savonius types of VAWTs [3,4,5,6].

Though HAWTs are believed to be more efficient than VAWTs for electricity generation in wind farms, evidently, it has not been proven beyond doubt that HAWTs are better than VAWTs in terms of performance when compared on equal scale. However, VAWTs may have inherent advantages over the HAWTs which have increased interest in research into small scale VAWTs in recent time:

(1) The rotor shaft is vertical and placed near the ground so a shorter tower is needed
(2) The generator and the gearbox can be placed near the ground which makes maintenance easier.
(3) The blades can be made of symmetrical aerofoils without twist and taper which make them easier and cheaper to manufacture.
(4) It does not need yawing mechanism
(5) Lower sound emission because of lower blade speeds
(6) Better performance in turbulent air flow when compared to HAWTs, this makes them usable in areas where tall devices are prohibited by radar laws [7].

The unsteady nature of VAWTs as it undergoes rotational motion has made the understanding of its flow characteristics complex especially at lower tip speed ratios. This may be due to rapid changes in azimuth angle and so angle of attack as the blade completes its cyclic motion. This complex flow phenomenon exhibited by VAWTs is largely dependent on the design parameters. El–Samanoudy et al [7] demonstrated experimentally that varying pitch angle, number of blades (so solidity), aerofoil type, and turbine radius have significant effect on the performance of VAWTs.

Solidity, Reynolds number, tips speed ratio, and blockage ratio are other design parameters that influence the performance of wind turbines. Good understanding of the influence of each will not only assist research in explaining the aerodynamics and performance of VAWTs, but will also influence the choice of aerofoil geometry which has a direct impact on the cost and economic viability of wind turbines. This paper seeks to investigate the effects of one non–dimensional group on the aerodynamics of VAWTs; solidity. Solidity is the ratio of the total projected area of a blade to the area swept out by the blade as it rotates. Equation 1 is an expression of solidity where N = number of blades, c = chord length and r = turbine rotor radius.

$$\sigma = \frac{N c}{r} \tag{1}$$

This study investigates the effects of solidity on the performance of a three–bladed 5KW scale VAWTs with NACA0012 blade profile by changing the chord length of the aerofoil. Seven turbine configurations of chord lengths of 0.098m, 0.149m, 0.197m, 0.248m, 0.299m, 0.351m and 0.48m with corresponding solidities of 0.2, 0.3, 0.4, 0.5, 0.6, 0.7, 0.98, were investigated. The power coefficient (Cp) was computed over a wide range of tips speed ratios (λ) as in equation 2, where (v_b) is blade velocity and (v_w) is wind velocity, to capture a good trend of the turbine performance.

$$\lambda = \frac{v_b}{v_w} \tag{2}$$

2. METHODS

2.1 Numerical Method

The investigation was designed for a 2D computational domain. The three-straight bladed model was created to simulate flow through the turbine's cross section. The computational domain contained a small rotating sub-domain embedded within a 15d long and 10d wide regular stationary sub-domain (where d is the diameter of the turbine) (Figure 1a). The rotor has a diameter of 3m with corresponding chord lengths for the various solidities studied. The rotor also incorporated a 0.17m diameter central shaft. The stationary domain dimensions were determined after a number of simulations performed with successive increases in domain size to ensure that boundaries are far enough away from the turbine so they have no effect on moment coefficient and turbine performance. This is also to avoid boundary problems such as insufficient wake development.

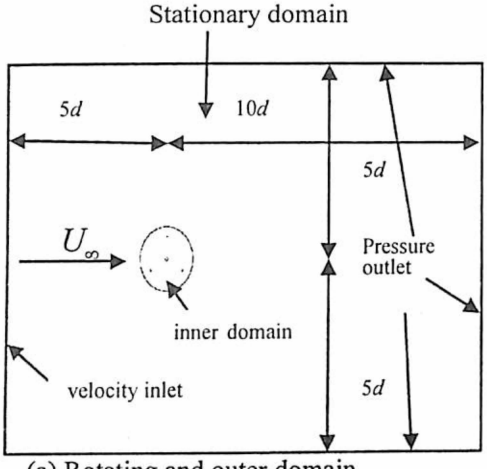

(a) Rotating and outer domain

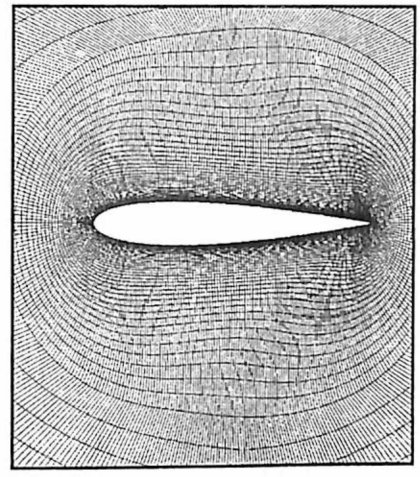

(b) 'O' mesh

Figure 1: Overview of the mesh around the aerofoil and geometry domain.

There is a sliding mesh interface at the boundary between the two sub–domains; the interface is 0.64m from the blades. To resolve the viscous affected region properly, each of the three aerofoils contained in the rotating domain is embedded in an O–mesh of 60 layers (Figure 1b), such that the refined O–mesh remained with the blades as the rotor sub–domain rotated relative to the outer stationary sub–domain. The entire domain contains a fully structured meshed and the boundary layer around the blades has a first cell height of 5e–06m which gives a range of y^+ of 0.8 $\leq y^+ \leq 5$ and an average of less than one from the flow solutions. The nodes are concentrated equally at both the leading and trailing edges for good capture of the flow physics. The 60–layer O–mesh around the aerofoils is inflated from the blade surface while the remaining rotating domain mesh is generated from the O-mesh, both with a growth rate of 1.1 The sharp trailing edge is rounded with an insignificant radius/chord ratio which has no effects on the results. The entire domain is approximately 148,000 cells.

Mesh sensitivity to changes in node number was performed by successively refining the aerofoil surface node density until there were insignificant changes in the torque coefficient from the flow turbine, a method similar to that of Hamada et al [8]. It has been observed that a finer mesh of 400 nodes provided similar results thus mesh independent was attained at this level. This is far less than the equally spaced node density of Amet et al [9] and Simao–Ferreira et al [10]. This investigation has been conducted with the commercial Computational Fluid Dynamics (CFD) package Fluent 12.1 [11]. The simulations were conducted with a flow of constant inlet velocity of 6.0m/s with turbulence intensity (Tu) of 1%. The flow is incompressible so a fully unsteady pressure–based coupled solver was selected and all the spatial discretization terms were set to second order.

The time step size was set to an equivalent of 0.5 degrees VAWTs rotation after time step size and convergence criteria sensitivity analysis was satisfied with negligible changes in torque. Based on the sensitivity analysis the time step convergence criteria were set to residual drop below 1x 10^{-4}. The simulations were allowed to run for ten full rotations within which periodic convergence was observed after five rotations (Figure 2).

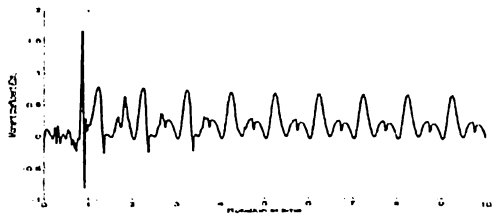

Figure 2. Periodic convergence of moment coefficient for a single VAWT blade..

2.2 Numerical Method Validation

Comparison of CFD numerical solutions to reference results (experimental results in most cases) authenticates the CFD model and influences the choice of turbulence models, level of solution accuracy and the computational time. Edwards et al [17' validated their models with a pitching aerofoil experiment data at a Reynolds number of 1.35 x 105; and they asserted that the dynamic interactions of a pitching aerofoil with a moving fluid are the closest possible validation cases versus static aerofoil data in the absence of VAWTs experimental data. The lift and drag plots (Figure 4,5) show SST k-ω model as the most suitable turbulence model for use in an unsteady aerofoil motion with dynamic stall characteristics.

The Novel Experimental Power Curve Determination and Computational Methods for the Performance Analysis of Vertical Axis Wind Turbines [17] also revealed SST k-ω model as the most appropriate model that predicted the dynamic shall behavior of their experiment results well. Though their study was at a low Reynolds number it confirms the results from other studies mentioned earlier and that of Martinat et al [13] and Ahmadi et al [14]. In general, these studies found out that the SST k-ω model produces results closest to experiment with respect to capturing the dynamic stall behavior and estimating the lift, drag and moment coefficient amplitudes. Based on these findings, and the close range of the Reynolds number to the present study, the SST k-ω model was used for the numerical simulations.

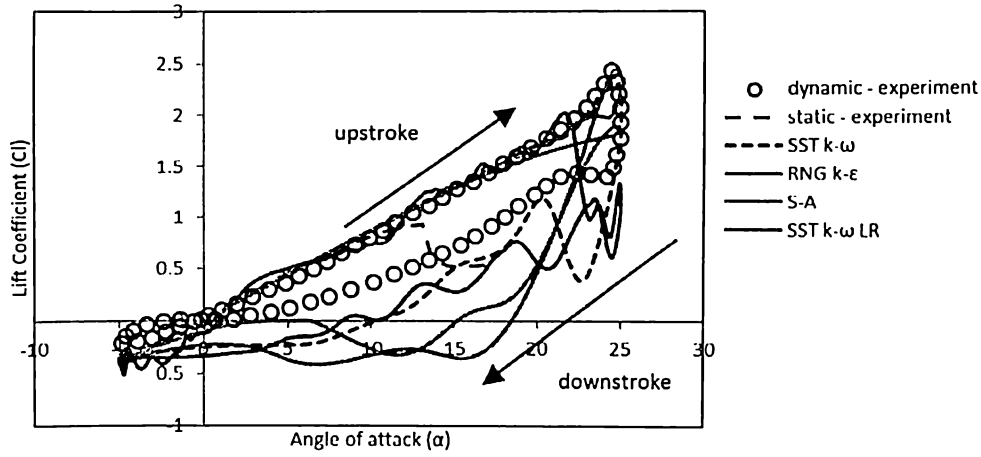

Figure 3: Lift coefficient loops with experiment data [17] for different turbulence models.

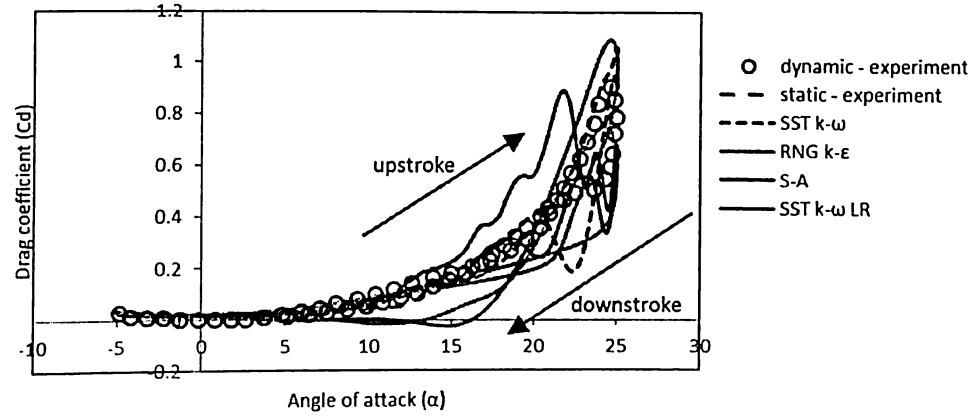

Figure 4: Drag coefficient loops with experiment data [17] for different turbulence models.

2.3 Energy Yield Method

Annual energy yield for the various turbine configurations was calculated for a site with wind speed distribution variation of ±30% and 6m/s annual mean speed. Based on the variation of the wind the average power and hence energy generated at each discrete wind speed is obtained, and the total energy that is generated in a year by each of the turbine configurations is calculated. This was based on the respective C_p–λ curves results from the solidity investigation (figure 5). Cut–in, rated, and cut–out wind speeds of 4m/s, 12m/s, 25m/s were considered. Using equation 2 the maximum and minimum tip speed ratio for fluctuations, of ±30% wind variation of the C_p–λ curve for the various solidities were established. The average aerodynamic power, the aerodynamic energy yield at each wind speed and hence total annual aerodynamic energy yield of the solidities were calculated.

To account for the seasonal and year-by-year variation of wind statistical data, a probability density function fitted into Weibull function was used [12]. This is defined by the following equations:

$$F(V) = \frac{K}{V}\left(\frac{V}{C}\right)^{k-1} \exp\left\{-\left(\frac{V}{C}\right)^{k}\right\} \quad (3)$$

Where $F(V)$ is the wind speed occurrence frequency, V is wind speed, C is the scale parameter and K is the shape parameter. Equation 3 was modified to give the probability of wind speed exceeding the value of V as:

$$P(V) = \exp\left\{-\left(\frac{V}{C}\right)^{k}\right\} \quad (4)$$

Where P(V) is the cumulative Weibull distribution. For this study k = 2 (because $k \neq 2$ makes the probability density distribution unimodal, that is the probability density is zero for discrete wind speeds close to zero.). This makes equation 4 a special Weibull distribution called Rayleigh distribution and $C = 1.13V_m$ where $V_{m,,}$ is annual mean wind speed. Based on wind speed 'bins' of 1m/s, the total hours in a year that the wind speed exceeds a discrete wind speed, V (discrete wind speed) was calculated by equation 5 and number of hours which power is generated at each discrete wind speed is extrapolated from the graph resulting from equation 5.

$$H = 8760\exp\left\{-\left(\frac{V}{C}\right)^{k}\right\} \quad (5)$$

From the simulations that ranged between the cut in and rated wind speed, the aerodynamic power is obtained for each discrete wind speed by equation 5 considering the range of λ for which the wind varies within ±30% of the annual mean wind speed, where $w_{\lambda 1}$ and $w_{\lambda n,}$ are turbine power, at the lower and upper limits of the tips speed ratios for the wind variation.

$$W_{ar} = \sum_{\lambda=1}^{n} \frac{(w_{\lambda 1} + w_{\lambda 2} + \ldots w_{\lambda n})}{N_{\lambda}} \quad (6)$$

The aerodynamic energy yield at each discrete wind speed is calculated using equation 7, where H_t is the number of hours the turbine operates at the discrete wind speed.

$$E_t = W_{ar} * H_t \quad (7)$$

And the annual aerodynamic energy yield for each of the solidity is calculated by equation 8.

$$E_{\sigma} = \sum_{t=1}^{n} (E_{t1} + E_{t2} \ldots + E_{tn}) \quad (8)$$

3. RESULTS

3.1 Solidity Effects on VAWT Performance

The performance curves in Figure 5 lie within a wide range of tip speed ratios (λ = 2-7) and show the effect of solidity by varying chord lengths from 0.098m – 0.48m. To understand the effects of solidity the torque and flow structures of cases $\sigma = 0.2$, $\sigma = 0.6$, and $\sigma = 0.98$ for one full rotation at $\lambda = 3$ were investigated. Figure 6 shows the torque history for the selected three solidities. The torque for $\sigma = 0.2$ peaks at $\theta = 78°$ and $\theta = 296°$ at the upwind section and the downwind section while $\sigma = 0.6$, and $\sigma = 0.98$ peaks lie close to $\theta = 100°$

and θ = 340° at the upwind and downwind halves. Case σ = 0.2 generate more negative torque at the upwind section that resulted in overall average torque of 3.95Nm/m followed by σ = 0.98 with an average torque of 4.37Nm/m while σ = 0.6 generate far less negative torque which contributed to an average torque of 9.78Nm/m. At the upwind section of the revolution, σ = 0.2 attained the lowest torque followed by σ = 0.98 and σ = 0.6 attained the highest peak while at the downwind section σ = 0.2 attained the highest torque followed by σ = 0.6 and σ = 0.98 attained the lowest torque.

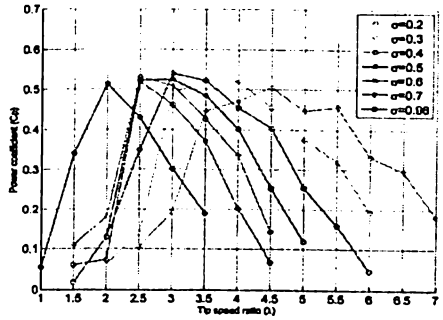

Figure 5: Effects of Solidity on C_p–λ for the seven turbine configurations.

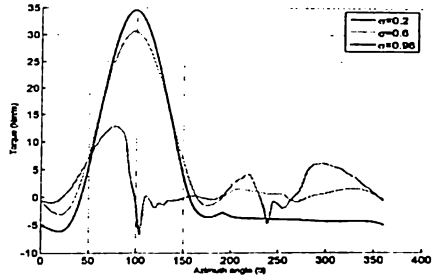

Figure 6: Comparing torque history of a blade for three solidities at λ = 3.

Significant difference is observed between the maximum torques attained in the two halves of the revolution. It is deducted from Figure 7 that the reduction in the maximum torque at the downwind section for the three solidities examined is due to the velocity induction in the upstream, the interaction of the blades with the blade's wake from the upstream half at the last quarter of the revolution around θ = 270°, wake blockage effects which reduces the free stream wind at the downstream half of the revolution and, solid blockage obstruction of the free stream velocity at the upstream half of the revolution.

Figure 7 also shows that increasing solidity increases the expansion of the stream tube as a result of the wake and solid blockage and these the blades at the downstream to see a lower velocity magnitude that results in lower lift to lower velocity as well as low flow incidence over the aerofoil.

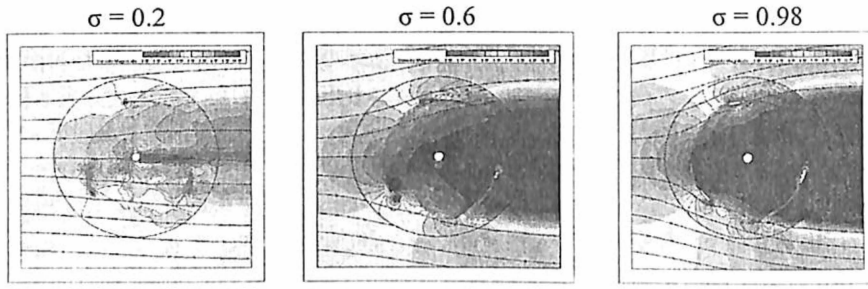

Figure7: Showing blade and wake interaction, and solid blockage λ = 3.

The blades of σ = 0.2 operate under stalled conditions for $\theta > 90°$ in the second quarter of the flow Figure 6. Figure 8 shows plots of vorticity for σ = 0.2, σ = 0.6, and σ = 0.98 operating at λ = 3 for the upwind section. Flow separation and vortex shedding is observed at $\theta = 100°$, $\theta = 120°$ and $\theta = 150°$ from the leading edge, trailing edge and the suction surface for σ = 0.2. This explains the low torque generated between $\theta = 100°$ to 190°, Figure 6. The flow is attached at the similar phase angle positions for σ = 0.6 and σ = 0.98 which explains the high torque generated between $\theta = 90°$ to 160°.

Figure 9 shows vorticity plots for the σ = 0.2, σ = 0.6, and σ = 0.98 operating at λ = 3 for the downwind half of the turbine. It is apparent that the flow for σ = 0.2 is still separated and there is also shedding of a pair of vortices from the trailing edge at $\theta = 240°$. This agrees with the findings of Fujisawa and Shibuya [16] that VAWTs shed two pairs of vortex for one complete blade revolution at low λ though their study was at lower Reynolds number. An onset of flow reattachment is observed at $\theta = 270°$ with almost reattached flow at $\theta = 290°$. However, the flow remain attached for σ = 0.6, and σ = 0.98 at similar phase position compared. This explains the superior power coefficient of σ = 0.6 and σ = 0.98 at λ = 3.

3.2 Energy Yield

To determine the turbine solidity with the overall best performance, the annual energy yield of the seven turbine configurations was investigated. To obtain the number of hours the turbine will operate in a particular wind speed in a year, a wind distribution with an annual mean wind of 6 m/s was assumed. Figure 10 shows the Weibull cumulative distribution of wind speed for a wind distribution with an annual mean wind speed of 6m/s from equation 4. Figure 11 shows the annual wind distribution for the site, constructed by calculating the percentage of each 1 m/s 'bins' and multiplying with the total numbers of hours in a year. It can be deduced from the Figure 11 that 6m/s discrete wind speed recorded the highest number of hours followed by 5m/s and 7m/s, and the number of hours for which the turbine operates after 15m/s is very low.

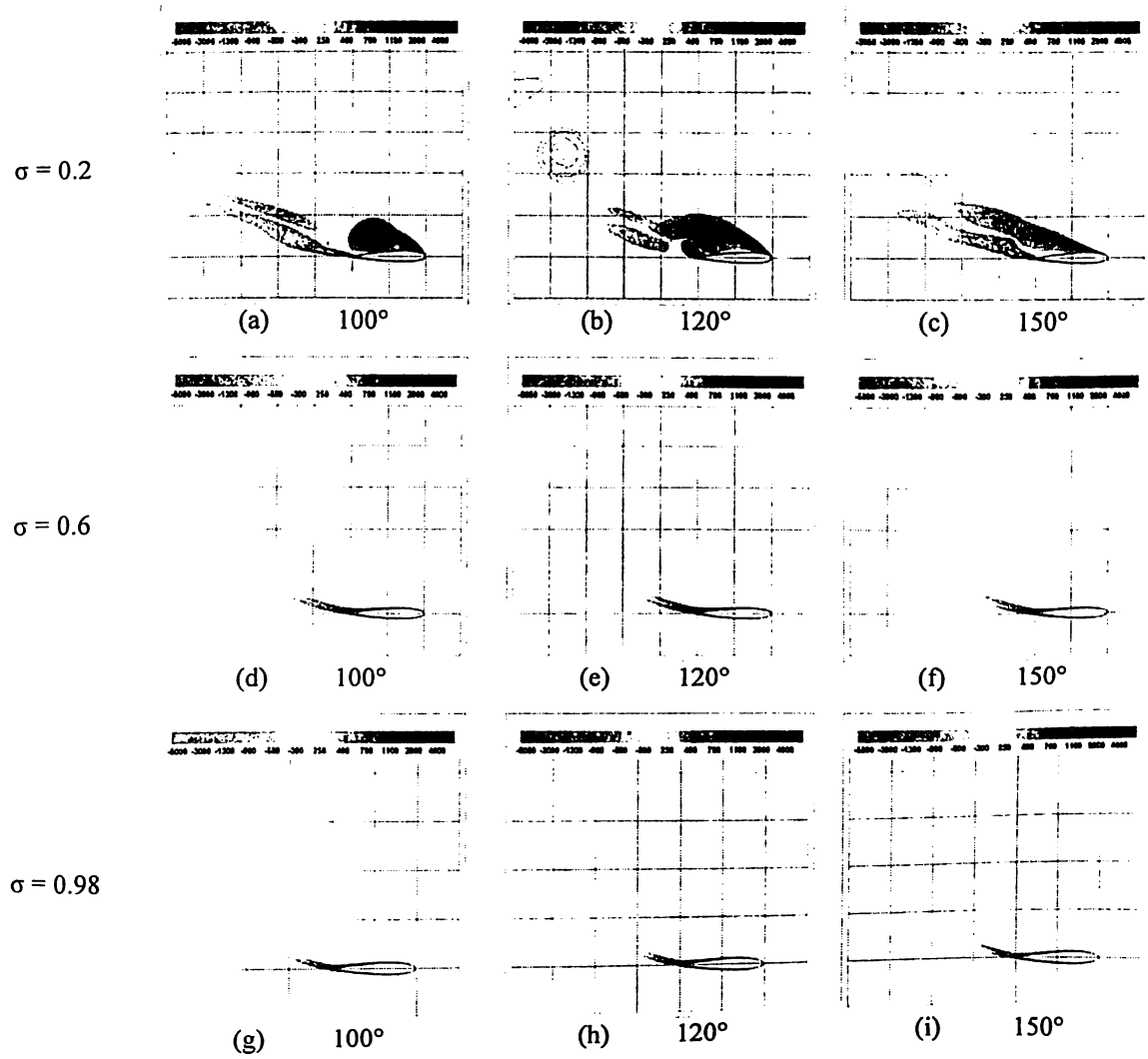

Figure 8: Comparing upwind flow features of a blade for three solidities at $\lambda = 3$ for different phase angles.

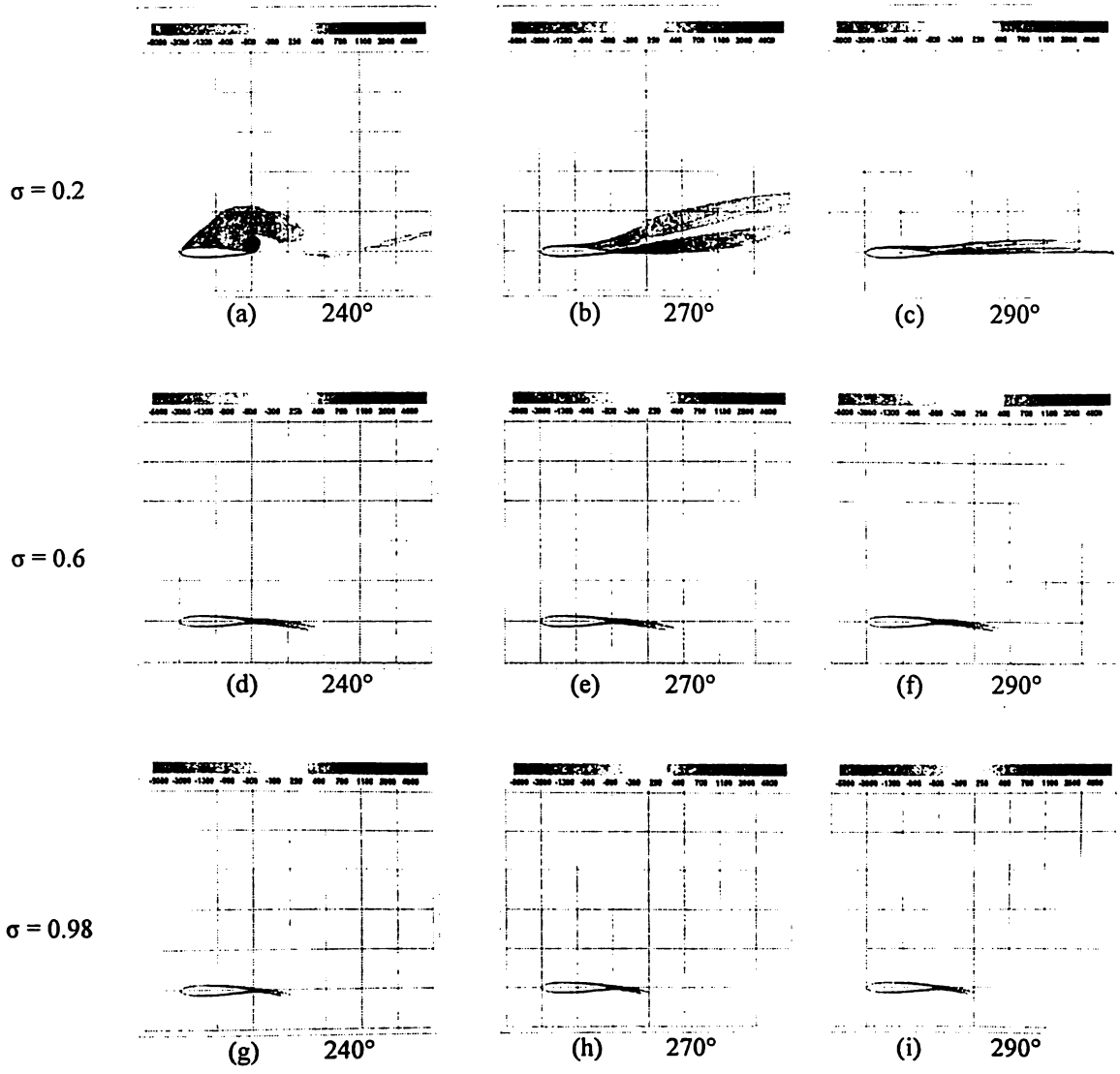

Figure 9: Comparing downwind flow features of a blade for three solidities at $\lambda = 3$ for different phase angles

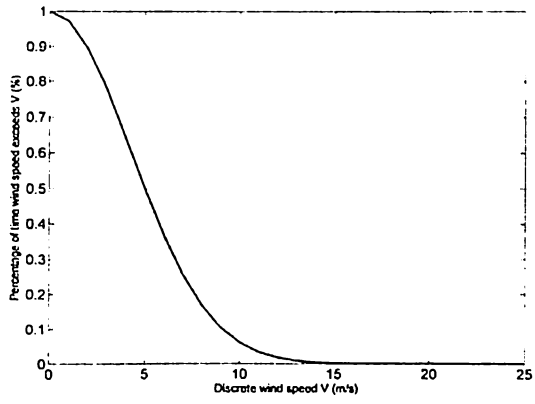

Figure10: Weibull cumulative distribution for 6m/s annual mean wind.

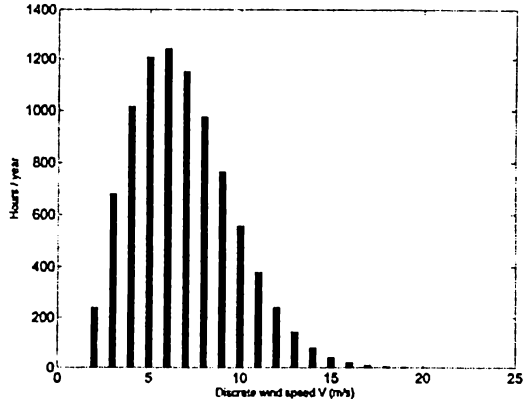

Figure 11: Annual mean wind speed distribution of generic site of 6m/s.

The power produced by each turbine solidity at a particular wind speed within the cut in wind speed of 4m/s, and rated speed of 12m/s for which simulations were ran, were extracted from the Fluent simulations and calculated using equation 7 depending on the range of λ within the ± 30% variation of the wind speed. For the low solidity, $\sigma = 0.2$, the turbine's power fluctuates around $\lambda = 3.46$ and $\lambda = 6.42$, while the turbine's power for the other low solidity, $\sigma = 0.3$ fluctuates around $\lambda = 2.69$ and $\lambda = 5$. And for solidity $\sigma = 0.4$ the turbine power fluctuates between $\lambda = 2.30$ and $\lambda = 4.28$. For $\sigma = 0.5$, 0.6 and 0.7 the turbines' power fluctuates between $\lambda = 1.92$ and $\lambda = 3.57$, while for the high solidity turbine, $\sigma = 0.98$, the power fluctuates between $\lambda = 1.53$ and $\lambda = 2.85$.

Figure 12 shows the annual aerodynamic power of the seven turbines configurations against wind speed. It shows that below 4 m/s, the cut in wind speed, the power produced by the turbine is negligible, also between 4 m/s and 12 m/s the power output rises rapidly and flattened out from 12 m/s. This is a typical characteristic variation of power against wind speed for wind turbines. The solidity turbines (σ = 0.3, 0.5 and σ = 0.4) produced the highest range of rated aerodynamic powers with σ = 0.3 producing the highest rated aerodynamic power of 7210 watts. This is followed solidity turbines (σ = 0.2, σ = 0.98, and σ = 0.6) and with case σ = 0.7 producing the lowest rated aerodynamic power of 5800 watts. It can be deduced from figure 12 that the influence of altering chord length on the turbine performance does not follow a sequential order but depends on performance curve characteristic and the fluctuation regime which the turbines operate.

Using equation 7, the aerodynamic energy yield produced at each discrete wind speed is calculated by multiplying the hours for each 'bins' discrete wind speed (Figure 11) by the turbine aerodynamic power at each 'bins' wind speed (Figure 12). And the annual aerodynamic energy yield is calculated using equation 9. It should be noted that high power production for a longer time leads to higher energy yield whereas high power production for a shorter period yields lower energy. Figure 13a and b shows the energy yield variation against discrete wind speed for the seven turbine configurations. σ = 0.3 marginally attained the highest energy yield followed by σ = 0.5 and the least is σ = 0.7. It can be deduced from Figure 13b that all the solidities attained their highest energy yield at a discrete wind speed of 9 m/s. However, the same trend is repeated by all the configurations as in Figure 14 with σ = 0.3 producing the highest aerodynamic energy yield, followed by σ = 0.5 and σ = 0.4. The low solidity σ = 0.2 performed optimally with σ = 0.7 recording the lowest aerodynamic energy yield. σ = 0.3 yielded the highest annual aerodynamic energy because of better aerodynamic performance of the blade (in terms of lift, drag and toque) as it interacts with wind speed, and also its performance was not too affected by the as the wind fluctuates between ±30 % . Solidities greater than or less than 0.3 based on chord lengths investigated in this study are characterized with less aerodynamic performances compared to σ = 0.3 though marginal performance differences were observed between σ = 0.3, and σ = 0.5 and σ = 0.4 as evidently shown in Figure 14, solidity = 0.3 is adjudged the best solidity based on the performance trend shown in this investigation.

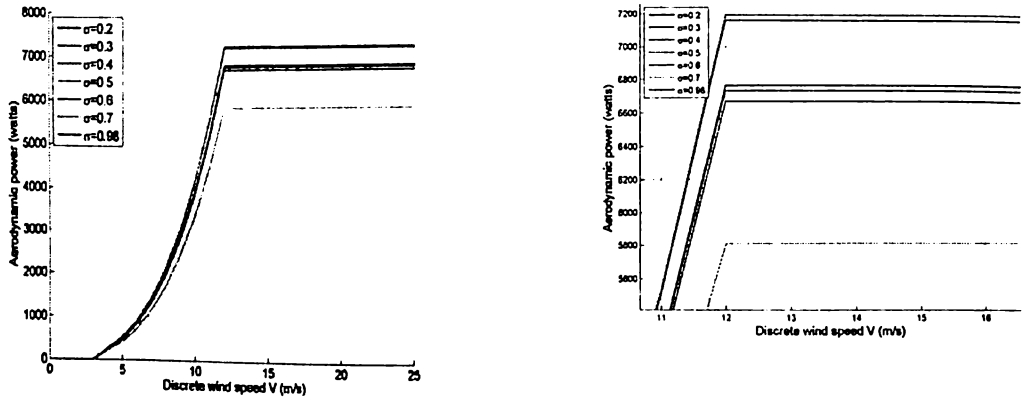

Figure 12. (a) Comparing annual aerodynamic power of the seven turbine configurations, (b) zoomed in section of (a).

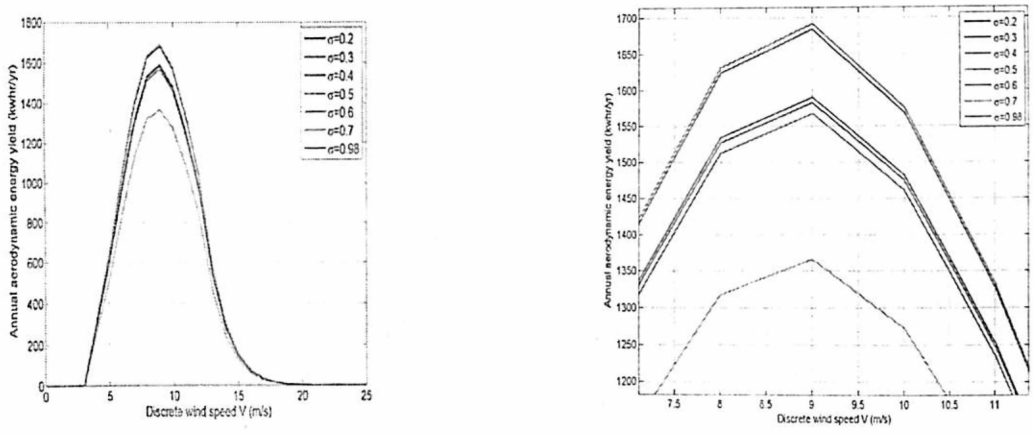

a. b.

Figure 13. (a) Comparing aerodynamic energy yield of the seven turbine configurations against discrete wind speed, (b) zoomed in section of (a).

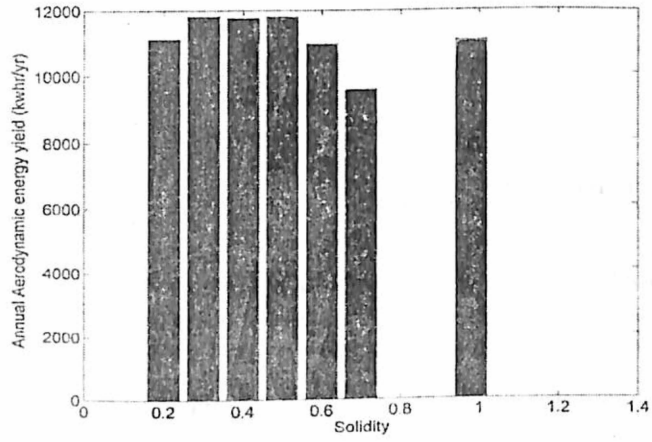

Figure14. Comparing annual aerodynamic energy yield of the seven turbine configurations.

4. CONCLUSIONS

The influences of solidity on the performance of seven VAWTs configurations have been investigated using CFD, and an annual energy yield method has been developed. Low solidity tended to increase the width of the bell shape region of the $C_p - \lambda$ curve whereas high solidity decreases the width of the $C_p - \lambda$ curve. Blade and wake interaction, solid and wake blockage, expansion of the stream tube, increase with increasing in solidity. This leads to reductions in velocity magnitude at the downwind pass of the blade and so lower power generation.

The high and medium solidity turbines attained their highest power coefficients at lower tip speed ratios whereas the low solidity turbine attained their highest power coefficients at medium tip speed ratios and all the solidities attained their highest aerodynamic energy yield at a discrete wind speed of 9 m/s for a wind speed distribution with annual mean wind speed of 6 m/s and variation of ±30%.Though $\sigma = 0.3$ yielded the highest rated aerodynamic power hence annual aerodynamic energy of all the solidities studied, it is worth mentioning that marginal differences in performance were observed in $\sigma = 0.3$, $\sigma = 0.4$ and $\sigma = 0.5$ for the wind fluctuation condition investigated.

ACKNOWLDGEMENT

For the funding provided for this research, Mr. Eboibi would like to thank the Tertiary Education Trust Funds (TETFunds) of Nigeria through the Delta State Polytechnic, Ozoro and Mr. Danao would like to thank the Engineering Research and Development for Technology Program of the Department of Science and Technology through the University of the Philippines' College of Engineering.

Nomenclature

μ	flow viscosity (N/m)	d	VAWT rotor diameter (m)
λ	tip speed ratio	F(v)	wind speed occurrence frequency
V_w	wind velocity	*Tq*	Torque (Nm/s)
C_m	coefficient of moment	CFD	Computational fluid dynamics
ρ	air density (kg/ms)	C_p	power coefficient
E_t	energy yield at discrete wind speed (kw)	NACA	national advisory committee on aeronautics
r	turbine rotor radius (m)	V	discrete wind speed
c	aerofoil chord length (m)	H_t	hours at discrete wind speed
N	number of blades	W_{ar}	aerodynamic power
σ	solidity of turbine	V_m	Annual mean wind speed
w_λ	power at tip speed ratio (watts)	E_{ar}	annual aerodynamic energy
P(V)	cumulative weilbull distribution	H	hours that wind speed exceeds 'V'
C	scale parameter	k	Shape parameter
Re_c	Reynolds number based on chord length	Tu	Turbulence intensity
HAWT	horizontal axis turbine	LR	Low Reynolds number
y^+	dimensionless wall distance	M	moment
VAWT	Vertical Axis Wind Turbine	SST	Shear Sress Transport

REFERENCES

1) ''UK energy in brief'' National Statistics Publication. URN 12D220. http://www.decc.gov.uk.
2) Beri, H., Yao Y. "Effect of Camber Airfoil on Self–Starting of Vertical Axis Wind Turbines." J. Environ. Sci. Technol., 2011, Vol 4.
3) "Vertical Axis Wind Turbine: The History of DOE Program". U.S Department of Energy, Sandia National Laboratories, America Wind Energy Association.
4) Dodd, H. H., Ashwill T. D., Berg D. E., Ralph M. E., Stephenson W. A., Veers P. S., "Test results and status of the DOE/Sandia 34–M VAWTS test bed." Proceedings of the Canadian Wind Energy Association Conference, September 14, 1989.
5) Dodd H. H., "Performance predictions for an intermediate–sized VAWTS based on performance of the 34m VAWTS test bed." Berg D. E. (editor), proceedings of the 9th ASME Wind Energy Symposium, Vol. 9, January 14–17, 1990.
6) Berg, D. E., Klimas P. C., Stephenson W. A., "Aerodynamic design and initial performance measurements for the Sandia 34–m vertical axis wind turbine." Proceedings of the 9th ASME Wind Energy Symposium, Vol. 9, January 14 – 17, 1990.
7) El–Samanoudy, M., Ghorab, A. A. E., Youssef, Sh. Z. "Effects of some design parameters on the performance of a Giromill vertical axis wind turbine" Ain Shams Engineering Journal., Vol. 1. Pp. 85–95., 2010.
8) Hamada, K., Smith, T., Howell, R., Qin, N., "Unsteady flow simulations and dynamic stall around vertical axis wind turbine blades." 27th ASME Wind Engineering Symposium, 2008 AIAA–2008–1319.
9) Amet, E., Maitre, T., Pellone, C., Achard, J. L., "2D Numerical Simulations of Blade – Vortex Interaction in a Darrieus Turbine". Journal of Fluids Engineering, 2009.
10) Simao–Ferreira, C. J. F., Bijl, H., Van Bussel G., Van Kuik, G. "Simulating Dynamic Stall in a 2D VAWT: Modeling strategy, verification and validation with Particle Image Velocimetry data" Journal of Physics 75, 2007.
11) Fluent 12 .1 User's Guide, 2010.
12) Jowder, F., "Wind power analysis and site matching of wind turbine generators in Kingdom of Bahrain". Applied Energy, 2009; 86: 538–45.
13) Martinat, G., Braza, M., Hoarau, Y., Harran, G., "Turbulence modelling of the flow past a pitching NACA0012 airfoil at 10^5 and 10^6 Reynolds numbers". Journal of Fluids and Structures 2008; **24**: 1294–1303. DOI: 10.1016/j.jfluidstructs.2008.08.002
14) Ahmadi, S., Sharif, S., Jamshidi, R., "A numerical investigation on the dynamic stall of a wind turbine section using different turbulent models". World Academy of Science, Engineering and Technology 2009; 58: 290–296.
15) Martino M., Aristide M., Antonio S., "Performances of vertical axis wind turbines with different shapes" Journal of Wind Engineering and Industrial Aerodynamics, 39, pp 83–93, 1992.
16) Fujisawa, N., and Shibuya, S., "Observations of dynamic stall on Darrieus wind turbine blades". Journal of Wind Engineering and Industrial Aerodynamics, 2000. 89(2001): Pp. 201–214.

17) Edwards, J, Danao, L. A., Howell, R., "Novel Experimental Power Curve Determination and Computational Methods for the Performance Analysis of Vertical Axis Wind Turbines". Journal of Solar Energy Engineering, 134(3), pp. 11.